Growth process and compressed phase of DMe-DCNQI on Ag(110) in the monolayer regime observed by LEED, XPS, and STM

C. Seidel,* H. Kopf, and H. Fuchs
Physikalisches Institut, Universität Münster, D-48149 Münster, Germany
(Received 18 September 1998; revised manuscript received 31 March 1999)

2,5-dimethyl-dicyanoquinonediimine films were grown on Ag(110) by organic molecular-beam deposition in an ultrahigh vacuum. During the preparation, the films were characterized *in situ* by low-energy electron diffraction. At distinguished stages of the preparation, x-ray photoelectron spectroscopy (XPS), and scanning tunneling microscopy (STM) were carried out. Two commensurate structures were found in two domain orientations. The first commensurate structure arose from a disordered arrangement (diffuse diffraction). At a certain substrate coverage, a second structure representing a compressed phase emerged from the first. In addition to the different unit cell sizes the structures differed in molecular orientation as verified by STM investigations. In addition to the major structural transitions, two minor modifications were observed. The XPS data indicate that in the monolayer regime an electron charge transfer occurs in all investigated structures from the metallic substrate to the molecule. [S0163-1829(99)03243-9]

INTRODUCTION

Organic molecules of the type of 2,5-dimethyl-N,N′-dicyanoquinonediimine (DMe-DCNQI) have recently attracted much attention because of their electronic and structural properties when forming radical ion salts.[1] A series of different counter ions like Cu, Li, Na, Rb, and K (Ref. 2) have been used previously. The anisotropic conductivity and its relation to external (temperature and pressure) and internal (deuteration) parameters of these charge-transfer crystals were the focus of former examinations.[3] Apart from these investigations performed on single crystals of $(\text{DMe-DCNQI})_x$ the growth on well-ordered crystalline surfaces brings about the possibility of producing new structures ranging from submonolayer to plurilayer or even thicker multilayer films, which are controlled by the metal surface. The commensurate growth of a DMe-DCNQI monolayer on Ag(111) and the chemical state of thicker films were examined by near-edge x-ray absorption fine structure and x-ray photoelectron spectroscopy (XPS) as reported by Bässler *et al.*[4]

The aim of this work was to investigate the growth process of DMe-DCNQI (shown in Fig. 1) on Ag(110) in the monolayer regime and to inspect different states of the preparation by XPS and scanning tunneling microscopy (STM). For this investigation a special low-energy electron diffraction (LEED) system was applied, allowing us to simultaneously record the diffraction pattern and the growth process.[5] We selected Ag(110) as a substrate because its low symmetry lets us expect homogeneous growth with a reduced amount of domain orientation compared with (111) or (100) oriented surfaces. Scanning tunneling microscopy (STM) was carried out to determine the local arrangement of the structures in real space. Our experiments allow a better understanding of the growth process and also provide some evidence for the existence of charge-transfer structures based on DMe-DCNQI.

EXPERIMENT

The experimental results presented here were obtained with two different ultrahigh vacuum (UHV) plants. The deposition of DMe-DCNQI and the simultaneous LEED measurements were performed at a residual pressure of 3×10^{-8} Pa. The special molecular beam deposition-LEED (Ref. 5) contains 3 sublimation cells with the DMe-DCNQI crucible tilted 22° from the normal to the surface. Function and resolution of the LEED optic (transfer width of 10 nm) correspond to a commercial three-grid system. Due to the low sublimation temperature of DMe-DCNQI at about 320 K (polymerization occurs at 340 K), the chamber was pumped for a prolonged period of time without being baked.

In the second chamber, we carried out XPS [with a hemispherical analyzer, CLAM II, vacuum generators (VG) using a twin anode (Mg $K\alpha$/Al $K\alpha$, XR3E2, VG)] and STM (STM/

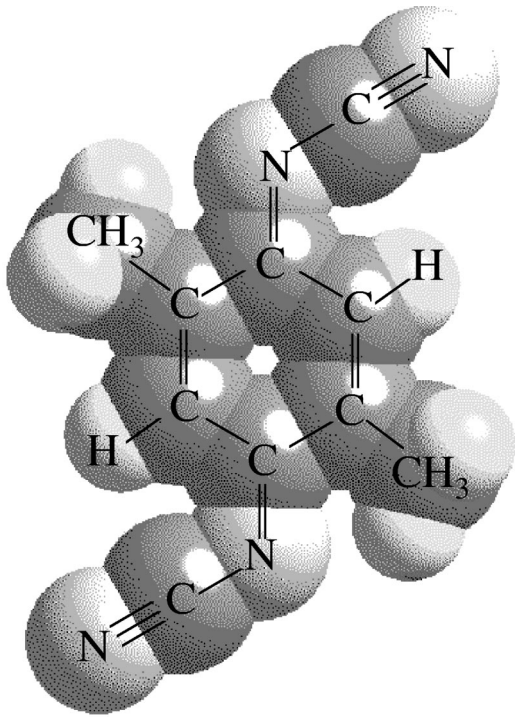

FIG. 1. Sphere model of the 2,5-dimethyl-N,N′-dicyanoquinonediimine.

SFM Omicron) investigations after taking additional electron diffraction images with a conventional LEED system to check the long range order of the DCNQI film. The second chamber was operated at a base pressure of 1.5×10^{-8} Pa. We used a differentially pumped evaporator introduced to the chamber via an air lock system, in this case allowing us to bake out the chamber. The purity and the sublimation rate of DMe-DCNQI were monitored by a mass spectrometer (BALZERS QMG 511). Crystal preparation was done by sputtering (500 eV Ar^+, $6\mu A/cm^2$, 20 min) and heating cycles (up to 700 K), and subsequently the samples were checked by LEED and XPS. Both preparation and film investigation could be carried out in either of the two vacuum plants without breaking the vacuum.

RESULTS

LEED experiments

The growth process was monitored by LEED *in situ* without changing the sample position. An example is shown in the diffraction images of Figs. 2(a)–2(i) presenting frames of a digitized series of images taken during film deposition. The images were taken at a substrate temperature of 315 K and at an electron energy of 14.6 eV. At the beginning, the DMe-DCNQI film causes a diffuse diffraction pattern [Fig. 2(a)]. At a higher dose sharp diffraction spots occur [Fig. 2(c)] corresponding to a single monolayer. After the first ordered structure is complete, a second type of structure forms [Fig. 2(f)], which is totally different from the first. Each of these structures exists in two domain orientations.

The first structure (in the following called monolayer or structure I) is determined relative to the substrate spots by $a_{1I}^*=6.56\,\mathrm{nm}^{-1}$, $a_{2I}^*=6.28\,\mathrm{nm}^{-1}$, while the second superstructure (in the following called structure II) is described by $a_{1II}^*=7.25\,\mathrm{nm}^{-1}$, $a_{2II}^*=7.3\,\mathrm{nm}^{-1}$. By using the substrate LEED patterns (not shown here) as well as the diffraction patterns of higher order, the reciprocal length can be given very precisely. In matrix notation the structures are described by

$$\text{structure I: DMe-DCNQI}\begin{pmatrix}+3&+1\\-2&+2\end{pmatrix}\text{Ag(110)},$$

Fig. 2(c)

with $a_{1I}=0.958$ nm, $a_{2I}=1.000$ nm, $\phi=100°$, area of a unit cell: 0.943 nm^2, and

$$\text{structure II: DMe-DCNQI}\begin{pmatrix}+3&+0\\+1&+2\end{pmatrix}\text{Ag(110)},$$

Fig. 2(f)

with $a_{1II}=0.867$ nm, $a_{2II}=0.866$ nm, $\phi=70.5°$, area of a unit cell: 0.708 nm^2. The two structures are shown in Fig. 3, which includes labels of characteristic spots and major crystallographic orientations.

Apart from the structural transition I→II during film growth, two additional transitions can be observed which are, for once, geometrical. Before the diffuse LEED images change to that of structure I, the position of the diffuse spots moves to higher k values in the [001] direction only. This behavior is shown in Fig. 4 by spot profiles of the (10) spot

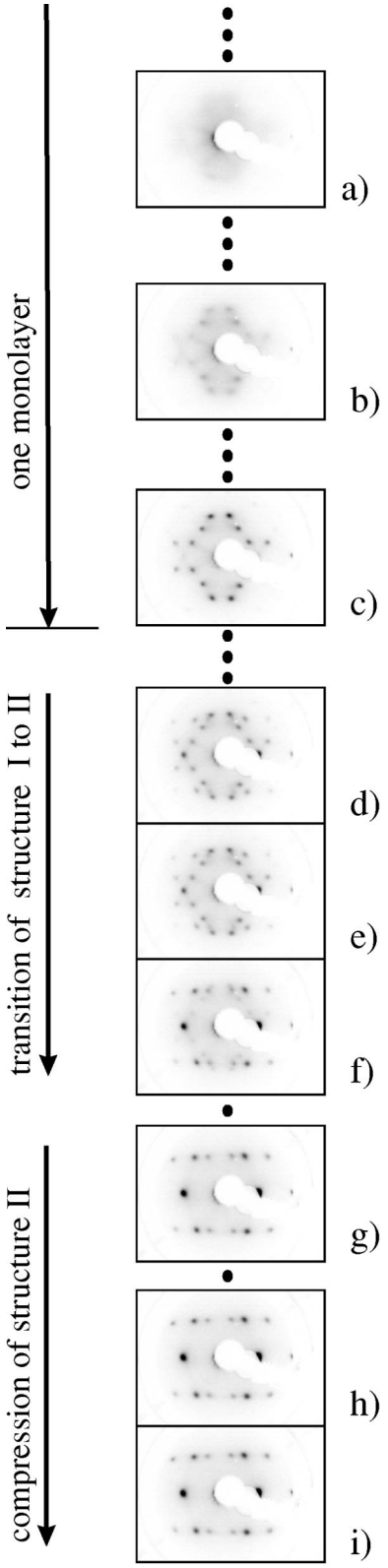

FIG. 2. Sequence of LEED ''film'' taken during preparation of the DMe-DCNQI. In this sequence, the development of the first structure (I) (image c) which is defined as one monolayer (1.1×10^{14} molecule/cm^2) and the transition into the second structure (II) (image f), 1.4×10^{14} molecule/cm^2 can be seen.

in directions [001] and $[1\bar{1}0]$ at an increasing DMe-DCNQI dose. In the [001] direction, i.e., along the rough profile of the surface, the spot distance changes by about 0.9 nm^{-1} in

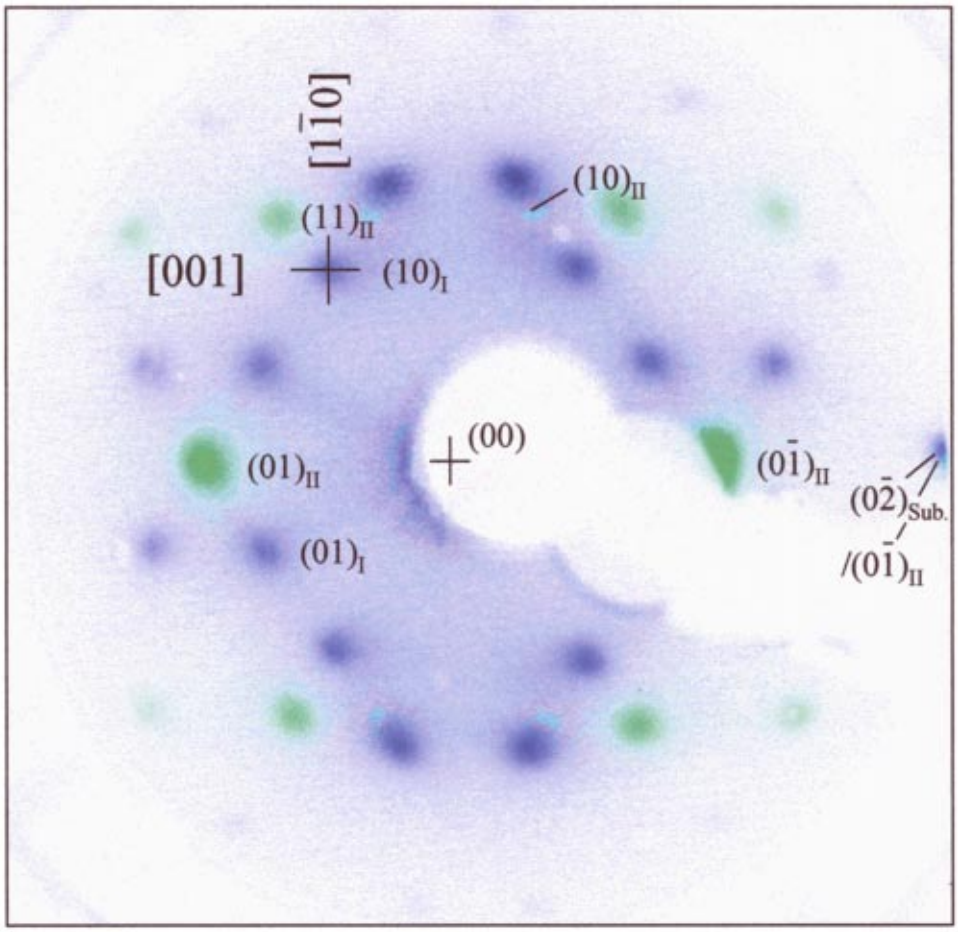

FIG. 3. (Color) Two specific images of the LEED picture series showing the different states during the preparation of the DMe-DCNQI. The blue-colored diffraction patterns show the first periodic structure (I), and the green diffraction patterns the second state (II). The LEED images were taken at an electron energy of 14.6 eV.

contrast to the smooth direction [1$\bar{1}$0] of the Ag surface, where the position of the spot does not change. The LEED images show that the development of structure I starts from a large unit size of 1.23 nm^2 with unit vectors of $a_{1I}=1.02$ nm, $a_{2I}=1.21$ nm, and an enclosed angle of $\phi=87°$ [matrix notation: DMe-DCNQ($^{+3}_{-2}$ $^{+1.3}_{+2.6}$)Ag(110)].

After structure II is completed, it undergoes another structural change. Fig. 5 shows a color composition of three LEED images where structure II was exposed to an additional constant DCNQI deposition rate. In this case, a slight increase of the k vectors in [1$\bar{1}$0] direction can be observed.

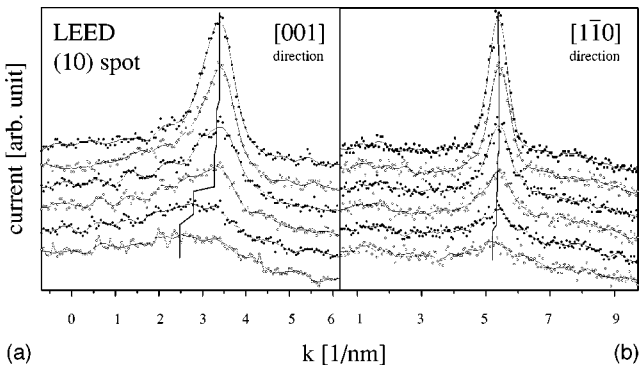

FIG. 4. Evolution of spot profiles of the (10) diffraction pattern of structure I in [001] (a) and [1$\bar{1}$0] (b) direction as a function of the DMe-DCNQI exposure (0.2×10^{14} molecule/cm^2 -1.06×10^{14} molecule/cm^2)

Figure 6 illustrates the spot position as derived from nine subsequent LEED images, partly shown in Fig. 2. The center of the (10) spots in [1$\bar{1}$0] direction change by about 0.25 nm^{-1}. Thus, in contrast to structure I, structure II seems to be compressed in the [1$\bar{1}$0] direction (smooth profile of the surface). The final structure ends with a small unit cell size of 0.637 nm^2 with the unit cell vectors of $a_{1I}=0.78$ nm, $a_{2I}=0.86$ nm, and an enclosed angle of $\phi=72.5°$ [matrix notation: DMe$-$DCNQI($^{2.7}_{0.9}$ $^{+1}_{+2}$)Ag(110)].

Photoelectron spectroscopy

Photoelectron spectroscopy was carried out to determine the molecular coverage and to document the C1s and N1s signal at different states of the preparation. In Fig. 7, 30 integrals of the C1s signal [sum of counts within the binding energy (BE) interval] are shown for different substrate coverages of DMe-DCNQI at two differing substrate temperatures (310 and 150 K). Here, the coverage is measured by the background subtracted sum of counts. In addition, the XPS signals of the multilayer were cleared of the self-attenuation effect. For each XPS measurement a corresponding LEED image was taken. As a result, Fig. 7 shows a linear relationship between the coverage and the exposure in the case of the cold substrate (150 K). Here, a diffuse LEED pattern was observed only at coverages of about 0.5×10^{14}/cm$^2-1.8\times10^{14}$/cm^2.

The same procedure was performed on a substrate maintained at 310 K. All structural transitions that took place

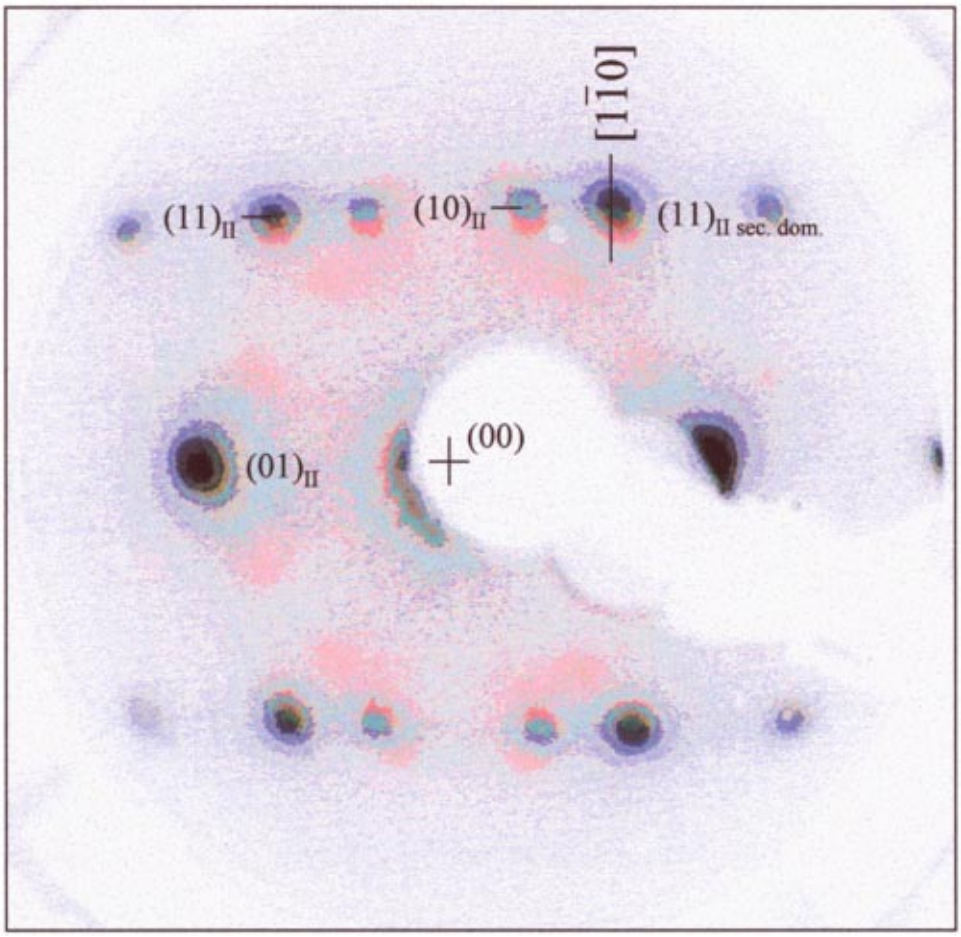

FIG. 5. (Color) The LEED sequence of structure II shows a small structural increase in the $[1\bar{1}0]$ direction. The green-colored diffraction patterns show the final state of the structure II. Electron energy: 14.6 eV.

showed the same dose-coverage relation as on a cold substrate until reaching the dose at which compression of the second structure is complete. Above this level, the dose-coverage ratio is reduced to 0.28 leading us to the conclusion that at low coverages the sticking probability is ~1, which is also confirmed by the fact that the coverage does not depend on substrate temperature.

The C1*s* and N1*s* XP spectra of the monolayer (structure I), the compressed monolayer (structure II), and a multilayer (14 nm thickness) are shown in Fig. 8. The spectra were recorded at 30 eV pass energy, resulting in an energy resolution of about 1.5 eV. The spectra were background subtracted in different ways: A linear background subtraction

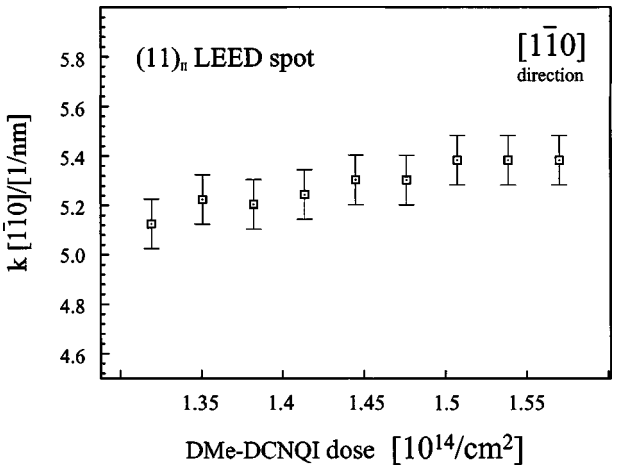

FIG. 6. Compression of the structure II in $[1\bar{1}0]$ direction.

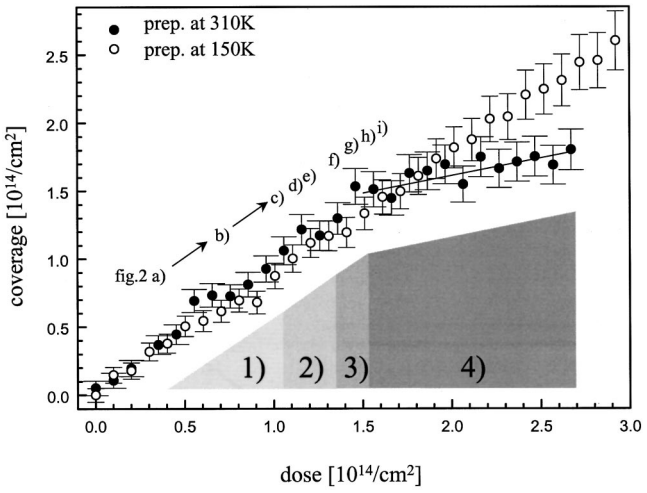

FIG. 7. Relation between DMe-DCNQ doses and coverage. The gray-shaded areas mark the different states of superstructures which are documented by LEED: (1) up to a monolayer, (2) transition from structure I (monolayer) to II, (3) compression of structure II, (4) growth without significant change in the diffraction pattern.

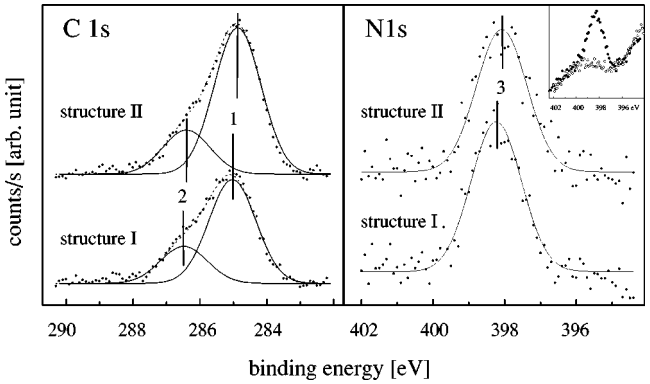

FIG. 8. XPS C1*s* and N1*s* spectra of a multilayer DMe-DCNQI, the monolayer (structure I) and the compressed monolayer (structure II).

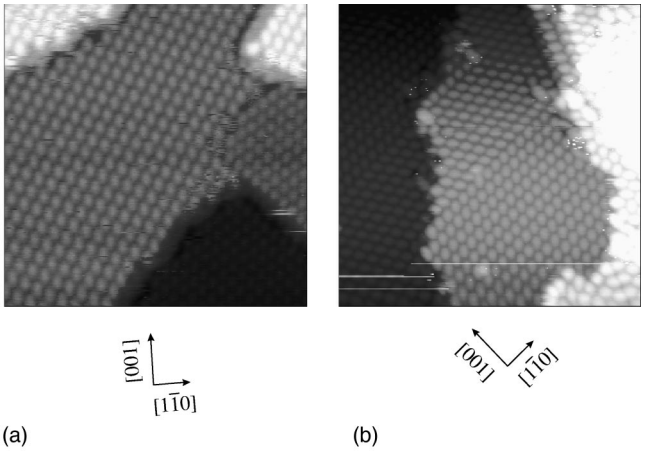

FIG. 9. Raw STM images showing the first and second adsorbate structures in their two domain orientations. Scan parameters are: 20 nm×20 nm, (a) $I_T=10$ pA, $U_T=0.7$ V, (b) $I_T=19$ pA, $U_T=1.44$ V.

was applied to the C1*s* and the multilayer N1*s* spectra. The N1*s* spectra of structure I and II were background subtracted by using the (structured) spectra of the clean silver surface. Here, the damping of the photoelectron signal was taken into account. According to the electron densities of the structures compared with graphite, a damping of 9% and 12% for structures I and II is estimated, respectively.

The C1*s* spectrum of the multilayer contains two peaks [BE 284.8 eV (labeled 1) and 286.6 eV (labeled 2)]. According to Refs. 4 and 6 these peaks can be assigned to the aliphatic or quinone state (labeled 1) and partly to carbon from the cyano and imino group (labeled 2), respectively.

The C1*s* XP spectra of the monolayer structures I and II obviously contain two peaks, the signal intensity of peak 2 being rather small. Here, the binding energy of the C1*s* core level of structure I is 284.5 eV (labeled 1) and 285.8 eV (labeled 2) and for structure II 284.2 eV (labeled 1) and 285.6 eV (labeled 2). The fits of the C1*s* spectrum should reflect the chemical state of the film in two regions. The fits were carried out by using Gaussian functions, the only constant setting being the linewidth (1.5 eV) according to the resolution of the analyzer, which was determined by the pass energy (30 eV) and the natural linewidth of the source (about 0.9 eV).

As expected from the structural data, the total signal intensity of the C1*s* signals of structure II is 34.5% (expected: 33%) higher than that of structure I.

Changes similar to the C1*s* spectra are observed in the N1*s* signals. In the multilayer regime two peaks separated by 0.8 eV and attached to the cyano and imino nitrogen can be identified. The peak ratio is about 1. In contrast, only one peak is observed in the N1*s* spectra of structures I and II. The corresponding binding energies are 398.3 eV (I) and 397.95 eV (II). The signal intensity of structure II is not exactly 33% higher than that of structure I. A maximum of +29% was observed as a result of several preparations. The reason for this seems to be that cyano and imino nitrogens are more easily deteriorated by x-ray than the quinone and methyl carbon.

STM investigations

STM images were taken separately after preparing structures I and II. Figure 9(a) shows an image 20 nm×20 nm in size where the two different oriented domains of the structure I were obtained on silver terraces. The STM images were taken at a tunneling voltage of 0.7 V (tip positive) and a tunneling current of 10 pA. Figure 9(b) shows the second superstructure (structure II) at the same scan size of 20 nm ×20 nm. In this second structure, the molecules are obviously more densely packed than in structure I. This observation supports the LEED results. The orientation of the substrate is shown at the bottom of the STM images. This information was taken from the LEED images of the uncoated Ag(110) surface and the known scan direction of the STM. The STM images provided the following data (averaged over the two domains):

$$\text{structure I: } a_{1\text{I}}=0.96\,\text{nm},\ a_{2\text{I}}=0.90\,\text{nm},\ \phi=96°,$$

$$\text{structure II: } a_{1\text{II}}=0.81\,\text{nm},\ a_{2\text{II}}=0.76\,\text{nm},\ \phi=77°.$$

These values differ by about 10% from the structural data obtained from the LEED measurements. At the chosen tunneling parameters, where the tip is located relatively far away from the surface, the shape of DMe-DCNQI molecules appear as ovals without any internal structure. Only these tunneling conditions (0.7 V, 10 pA) enabled us to obtain stable images. Submolecular resolution could not be achieved.

An overview of the preparation steps and the analytical measurements performed on DMe-DCNQI/Ag(110) is shown in Table I. The results presented in this paper are marked.

DISCUSSION

The discussion of structural and spectroscopic results are separated into four sections.

Commensurate structures

At two different states of preparation (coverage and substrate temperature) we found clearly periodic structures resulting in sharp LEED patterns (Figs. 2, 3, and 5) and molecularly resolved STM images (Fig. 9). The LEED

TABLE I. Survey of investigations of Me-DCNQI on Ag(110). ■, Presented here; □, measured.

	Submonolayer	Structure I (monolayer)	Structure II	Compressed Structure II	Multilayer
MBD-LEED	■	■	■	■	□
STM[a]		■	■		
XPS[b]	□	■	■		■
sticking coef.[b]	■	■	■	■	■

[a]LEED checked.
[b]MBD-LEED checked.

calculation shows that these structures are commensurate, (as related to the substrate patterns) existing in two domain orientations (symmetry of the LEED pattern). Due to time-dependent distortions (temperature and voltage dependent elongation of the STM scanner) we did not use the STM images to determine the unit vectors of the adsorbate. Nevertheless, the STM data coincide within a 10% margin with those of the LEED data. The absence of long-range modulation in the STM images (a multiple of the adsorbate unit vectors causing moiré structures) supports the interpretation of both structures I and II as being commensurate. The use of the moiré technique to distinguish between a coincidence and a commensurate structure was demonstrated by Hoshino *et al.* using PTCDA on graphite.[7] A growth in two domain orientations can be expected on a substrate of *pmm* symmetry with the adsorbate structure breaking the mirror symmetry of the substrate.

The two-dimensional symmetry group of the two adsorbate structures marked green and blue in Fig. 3 belongs to the $p1$ group as can also be concluded from the STM images. In addition, the LEED does not indicate a complex unit cell because of the monotonic decrease in spot intensity from low- to high-order spots seen in the LEED images at higher electron energies.

Following this interpretation, the area for one DMe-DCNQI molecule (and for the unit cell of the adsorbate) is 0.943 nm^2 for structure I and 0.708 nm^2 for structure II. This means that the same area of structure II contains 33% more DMe-DCNQI molecules than structure I. In Fig. 10 a model for the two commensurate structures (marked with black unit vectors) are shown. It has to be kept in mind, though, that the absolute positions of the molecules shown in Fig. 10 are hypothetical, as the substrate atoms they could not be determined directly via STM.

Structural transitions

During film preparation we found three structural transitions: During the first transition, occurring in [001] direction, the $(10)_I$ spot changes its position (like all its equivalents) during film growth to higher k values. This can be interpreted as a compression of a large superstructure to create the commensurate structure I. In parallel to this, the half width of this spot changes significantly during preparation in [001] but not in $[1\bar{1}0]$ direction (Fig. 4). This change of the spot size might be caused either by varying the length of the unit cell in [001] direction or by DMe-DCNQI islands, the extensions in [001] direction of these islands being comparable to the transfer length of the LEED (about 10 nm). This means that changes in the island's size change the size of the LEED spots.

The transition from structure I to structure II also seems to be driven by the increasing amount of DMe-DCNQI deposited. The transition occurs at a molecular coverage slightly over a monolayer (about $1.05-1.3\times10^{14}/cm^2$).

The third structural transition occurs after structure II is complete. Here, in contrast to the first structural transition, the k vector in $[1\bar{1}0]$ direction increases by about 0.25 nm^{-1} while the surface is being exposed to a constant DMe-DCNQI deposition rate from the gas phase. In real space, this corresponds to a compression of 0.06 nm parallel to the silver rows. In Fig. 10, the two main commensurate structures (unit vectors and molecules marked in black) as well as the incommensurate precursor and final structures (marked in gray) are shown. In addition to the unit vectors, a suggested orientation of the molecules found with the STM images is presented. Another difference between the two structures is evident on the border between the domains. Structure I does not match its mirror plane structure [shown in Fig. 9(a)], in contrast to structure II where the border fits the two domain structures. This is caused by the orientation of one of the unit vectors of structure II, which is parallel to the $[1\bar{1}0]$ direc-

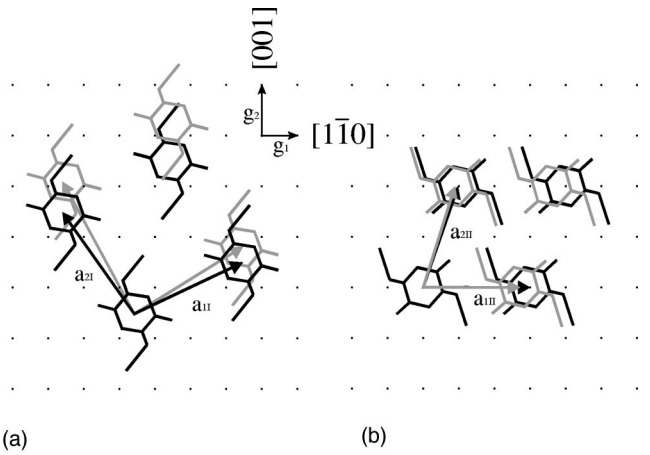

FIG. 10. Real space model of the two major structures (I, II) and their precursor and final state respectively. The unit vectors were obtained from LEED and STM data, the orientations of the molecules were taken from STM images only. Changes in the unit cells of the precursor structure of structure I and the final state of structure II are given by molecules drawn in gray. The absolute position of the molecule relative to the substrate shown has not yet been confirmed experimentally.

tion. In the STM images, the molecules appear as oval-shaped dots without any internal structure. Considering that the charge transfer electron is probably located near the cyano and imino groups rather than near the methyl groups, the long axis of the oval profile in the STM images should correspond to the DMe-DCNQI axis which is defined be the cyano group. Regardless of this, the molecules of structure I are azimuthally oriented 90° relative to the $[1\bar{1}0]$ direction, and those of structure II by 25°. During the transition from structure I to structure II, all molecules rotate by 65°.

We believe that this orientation explains the different directions in which the compressions occur within structures I and II. In both cases, the compression occurs along the long axis of the DMe-DCNQI molecules, where the cyano groups terminate the molecule. In bulk charge transfer complexes,[1,8,9] these cyano groups are the reactive part and are responsible for the coordination of the molecules. In contrast, the methyl sites of the molecules do not allow any reaction with the substrate or a neighboring molecule and can act only by steric effects. Apart from the influence of the substrate to build up certain superstructures, it also seems that the reactive part of the molecule plays an important role for the observed structures.

Photoelectron spectroscopy

The XPS 1*s* signals of the carbon and the nitrogen show a significant difference between the multilayer structure and the monolayer or compressed monolayer structures. In the multilayer structure, which shows the pure DMe-DCNQI without a substrate effect (14 nm thickness), the two peaks can be associated with the cyano carbon (BE 286.6 eV), the C atoms of the quinone ring, and the methyl group (BE 284.8 eV). This interpretation leads to an expected stoichiometry of 1:4, differing from the measurement in which a relation of 1:1.2 was found. The difference is probably caused by satellites of the chinone ring that increase the signal intensity at higher binding energies. In contrast to the multilayer spectrum, the C1*s* spectra of structures I and II show a reduced peak at higher binding energy (Fig. 8, label 2), indicating a change in the electronic structure. This change might be caused by a partial charging of the molecule (charge-transfer reaction) possibly reducing the satellite intensities. In addition to this effect, an improved electronic screening of the core hole might reduce the binding energy and the satellites. Additional XPS measurements of a monolayer of DMe-DCNQI on Au(111) have been recently carried out. Here, the C1*s* spectrum correspond to the (not reacted) multilayer spectra shown in Fig. 8 indicating that the molecules are definitely not reacted. This supports the interpretation that the difference between the multilayer spectrum and the monolayer and compressed monolayer spectra on Ag(110) cannot be completely explained as a (collective) charging by the 5*s* electrons of the metal.

The N1*s* spectra show a behavior similar to that of the C1*s* spectra. The two peaks in the multilayer regime seem to be merged into single peaks in structures I and II and occur at lower binding energies.

The XP spectra show that no monotonic relation between coverage and binding energies exists because the binding energy is lowest for the compressed monolayer structure. Therefore, we believe that the charging of the adsorbate strongly depends on the local orientation of the DMe-DCNQI molecules relative to the substrate.

CONCLUSIONS

During growth of a DMe-DCNQI in the monolayer regime on Ag(110) three structural transitions (compression's) were observed, depending on the coverage. Surprisingly, the first compression occurs along the rough direction of the Ag(110) surface, while the second represents a transition between two commensurable structures. The third transition is a compression along the smooth profile of the (110) surface. These transitions can be uniformly explained by considering a cooperative rotation of the organic molecules during the second transition. As a result, all transitions occur along the long axis of the molecule. Taking into account that the long axis is terminated with the reactive cyano groups the transitions can be understood as a coordination of the molecules by the Ag atoms in a similar way to the building of (3*d*) single-crystal charge-transfer complexes. Control experiments performed on Au did not show this effect. The growth was documented by a special LEED system which allowed simultaneous recording of the diffraction patterns during evaporation. In addition, STM measurements at different preparation states allow us to document the different orientation of the molecules locally. The XPS measurements indicate that a charge transfer takes place in all (submonolayer, monolayer, and compressed monolayer) structures.

ACKNOWLEDGMENTS

The authors would like to thank Dr. J. U. von Schütz, University of Stuttgart, and Professor S. Hünig, University of Würzburg, for providing the DMe-DCNQI material and Professor N. Karl and Dr. U. Zimmermann for making the LEED software available for calculatung the LEED images.

*Author to whom correspondence should be addressed. FAX: ++49 251 833 3602. Electronic address: seidelc@nwz.uni-muenster.de

[1] G. D. Andretti, S. Bradamante, P. C. Bizzari, and G. A. Pagan, Mol. Cryst. Liq. Cryst. **120**, 309 (1985).
[2] S. Hünig and P. Erk, Adv. Mater. **3**, 225 (1991).
[3] H. Wachtel, Synth. Met. **54**, 363 (1993).
[4] M. Bässler, R. Fink, C. Heske, J. Müller, P. Väterlein, J. U. von Schütz, and E. Umbach, Thin Solid Films **284-285**, 234 (1996).
[5] C. Seidel, J. Poppensieker, and H. Fuchs, Surf. Sci. **408**, 223 (1998).
[6] H. Kopf, C. Seidel, and H. Fuchs, Thin Solid Films **342**, 307 (1999).
[7] A. Hoshino, S. Isoda, H. Kurata, and T. Kobayashi, J. Appl. Phys. **76**, 4113 (1994).
[8] R. Kato, H. Kobayashi, A. Kobayashi, T. Mori, and H. Inokuchi, Chem. Lett. **8**, 1579 (1987).
[9] A. Aumüller, P. Erk, G. Klebe, S. Hünig, J. U. von Schütz, and H. P. Werner, Angew. Chem. Int. Ed. Engl. **25**, 740 (1986).